The Influence of Atmospheric Cloud Radiative Effects on the Large-Scale Atmospheric Circulation

YING LI AND DAVID W. J. THOMPSON

Department of Atmospheric Science, Colorado State University, Fort Collins, Colorado

SANDRINE BONY

Laboratoire de Météorologie Dynamique, IPSL, CNRS, Université Pierre et Marie Curie, Paris, France

(Manuscript received 5 December 2014, in final form 13 June 2015)

ABSTRACT

The influence of clouds on the large-scale atmospheric circulation is examined in numerical simulations from an atmospheric general circulation model run with and without atmospheric cloud radiative effects (ACRE). In the extratropics of both hemispheres, the primary impacts of ACRE on the circulation include 1) increases in the meridional temperature gradient and decreases in static stability in the midlatitude upper troposphere, 2) strengthening of the midlatitude jet, 3) increases in extratropical eddy kinetic energy by up to 30%, and 4) increases in precipitation at middle latitudes but decreases at subtropical latitudes. In the tropics, the primary impacts of ACRE include 1) eastward wind anomalies in the tropical upper troposphere–lower stratosphere (UTLS) and 2) reductions in tropical precipitation. The impacts of ACRE on the atmospheric circulation are interpreted in the context of a series of dynamical and physical processes. The changes in the extratropical circulation and precipitation are consistent with the influence of ACRE on the baroclinicity and eddy fluxes of momentum in the extratropical upper troposphere, the changes in the zonal wind in the UTLS with the influence of ACRE on the amplitude of the equatorial planetary waves, and the changes in the tropical precipitation with the energetic constraints on the tropical troposphere. The results make clear that ACRE have a pronounced influence on the atmospheric circulation not only at tropical latitudes, but at extratropical latitudes as well. They highlight the critical importance of correctly simulating ACRE in global climate models.

1. Introduction

Accurate simulations of the atmospheric general circulation are a necessary condition for interpreting climate variability and predicting the climate response to external forcings. However, climate models exhibit a wide range of biases in their simulations of the current climate, and a major source of such biases stems from cloud processes and their role in the general circulation (e.g., Möbis and Stevens 2012; Ceppi et al. 2012; Oueslati and Bellon 2013; Stevens and Bony 2013). One of the ways clouds can affect the atmospheric circulation is through their influence on the radiative heating of the atmosphere.

Cloud radiative effects (CRE) have long been recognized to influence Earth's radiation budget. They have been quantified for decades at the top of the atmosphere (TOA; Ramanathan et al. 1989; Harrison et al. 1990; Hartmann et al. 1992; Loeb et al. 2009), and recent advances in remote sensing have made it possible to also quantify them at the surface and within the atmosphere (L'Ecuyer et al. 2008; Su et al. 2010; Allan 2011; Kato et al. 2011; Haynes et al. 2013). On the global scale, the net atmospheric cloud radiative effects (ACRE; defined as the difference in cloud radiative effects between the TOA and the surface) are surprisingly small due to the compensation between cooling due to low clouds at high latitudes and warming due to high clouds in the tropics. But on local and even synoptic scales, ACRE can readily reach several tens of watts per square meter. Since they contribute to atmospheric diabatic heating, ACRE can have a profound influence on the large-scale atmospheric circulation.

Corresponding author address: Ying Li, Department of Atmospheric Science, Colorado State University, 3915 W. Laporte Ave., Fort Collins, CO 80521.
E-mail: yingli@atmos.colostate.edu

DOI: 10.1175/JCLI-D-14-00825.1

Early studies using numerical simulations reveal that ACRE play a prominent role in determining the mean tropical circulation (Slingo and Slingo 1988, 1991; Randall et al. 1989; Gordon 1992; Sherwood et al. 1994; Tian and Ramanathan 2003). Other studies suggest that ACRE also play a role in tropical intraseasonal variability (Lee et al. 2001; Raymond 2001; Fuchs and Raymond 2002; Bony and Emanuel 2005; Zurovac-Jevtić et al. 2006; Crueger and Stevens 2015).

However, the influence of ACRE on the extratropical atmospheric circulation has received comparatively little attention. Those studies that have examined the role of clouds in the extratropical circulation have focused primarily on TOA radiative effects, particularly TOA shortwave effects. For example, Ceppi et al. (2012) argue that model biases in TOA shortwave cloud radiative forcing lead to biases in surface temperatures that induce biases in the latitude of the Southern Hemisphere midlatitude jet; Ceppi et al. (2014) suggest that trends in TOA shortwave cloud radiative forcing lead to trends in the midlatitude jet. Li et al. (2014b) argue that the TOA cloud radiative effects associated the northern annular mode act to shorten the time scale of its attendant temperature anomalies. Grise et al. (2013) and Grise and Polvani (2014) argue that changes in TOA cloud radiative effects associated with poleward shifts in the midlatitude jet can lead to significant global-mean warming in coupled climate models. For the most part, the physical mechanisms through which ACRE influence the large-scale extratropical atmospheric flow remain unclear.

Here we examine the influence of ACRE on the large-scale atmospheric circulation by analyzing numerical simulations performed under the auspices of the Cloud Feedback Model Intercomparison Project (CFMIP), in which clouds are made transparent to radiation. The simulations, referred to as the Clouds On-Off Klimate Intercomparison Experiment (COOKIE; Stevens et al. 2012), allow us to assess the impact that ACRE exert on the atmosphere for given surface boundary conditions. The COOKIE simulations include two primary types of experiments, both of which are run with an atmospheric general circulation model (AGCM) forced with the same observed sea surface temperatures: 1) control simulations that include model cloud radiative effects (''clouds-on'' experiments) and 2) perturbed simulations in which the model cloud radiative effects are turned off in the radiative computation (''clouds-off'' experiments). The differences between the clouds-on and clouds-off experiments reveal the impact of ACRE on the model climate.

As noted above, studies predating the COOKIE experiments have examined the role of cloud radiative effects on the atmospheric circulation, but have focused primarily on tropical latitudes (Slingo and Slingo 1988, 1991; Randall et al. 1989; Gordon 1992; Sherwood et al. 1994; Tian and Ramanathan 2003). Recent studies based on the COOKIE simulations have also explored the influence of cloud radiative effects on the atmospheric circulation, but in this case have focused on the radiative effects of boundary layer clouds on the tropical circulation (Fermepin and Bony 2014) or on the impact of ACRE on tropical intraseasonal variability (Crueger and Stevens 2015). Here we investigate the influence of ACRE imposed at all atmospheric levels and latitudes on the global atmospheric circulation, with an emphasis on the extratropics.

The paper is organized as follows: Section 2 reviews details of the COOKIE simulations, observations, and diagnostic techniques. Section 3 examines the long-term-mean, zonal-mean circulation in the control (clouds on) experiment. The impacts of ACRE on the model zonal-mean circulation are documented in section 4 and interpreted in section 5. Section 6 summarizes key results.

2. The COOKIE simulations, observations, and diagnostic approach

a. *The COOKIE simulations*

As noted in the introduction, the COOKIE simulations include two primary types of experiments: 1) control simulations run with ACRE (clouds-on experiments) and 2) perturbed simulations run without ACRE (clouds-off experiments). All other parameters are identical in the two types of simulations, including sea surface temperatures (SSTs). As such, the differences between the clouds-on and clouds-off experiments are due solely to the impact of ACRE on the model climate.

In the majority of the study, we will compare the long-term-mean, zonal-mean circulation between the clouds-on control simulation [referred to as the ''amip'' experiment in Stevens et al. (2012)] and a simulation where ACRE are turned off at all vertical levels [the ''offamip'' experiment in Stevens et al. (2012)]. Selected results will also draw from the following additional COOKIE simulations: 1) a 30-yr ''boundary layer clouds-off'' simulation [referred to as ''offpblamip'' in Stevens et al. (2012)], in which only planetary boundary layer clouds are made transparent to radiation; and 2) the 5-yr ''aquaplanet clouds-on'' and ''aquaplanet

clouds-off'' simulations [referred to as ''aquaControl'' and ''offaquaControl'' in Stevens et al. (2012)], which are identical to the clouds-on and clouds-off experiments, except that they are run in an aquaplanet configuration [see Stevens et al. (2012) for details].

Following the protocol from phase 5 of CMIP (CMIP5; Taylor et al. 2012), the clouds-on and clouds-off simulations are forced by observed monthly-mean SSTs and sea ice concentration over the 30-yr period 1979–2008. The absence of air–sea coupling complicates the comparison of the COOKIE output to the ''real world'' (e.g., Bretherton and Battisti 2000). However, the purpose of the idealized COOKIE simulations is not to reproduce the observed climate, but rather to understand how atmospheric heating perturbations associated with ACRE influence the atmospheric circulation for given surface boundary conditions. Similar frameworks are widely used to isolate the effects of other individual forcings on the climate system, for example, to disentangle the direct effects of increased CO_2 on the atmospheric circulation from the indirect effects due to the accompanying increases in sea surface temperatures (e.g., Deser and Phillips 2009; Bony et al. 2013).

The COOKIE simulations used in this study are run with the atmospheric component of L'Institut Pierre-Simon Laplace (IPSL) coupled climate model (version IPSL-CM5A-LR; Dufresne et al. 2013). The AGCM output is available on a 3.75° latitude × 1.875° longitude mesh and at 39 vertical levels (provided on a hybrid sigma pressure coordinate system). Details of the physics parameterizations used in the IPSL AGCM are provided in Hourdin et al. (2006).

b. Observations

The atmospheric circulation and cloud fields simulated by the IPSL model are compared with those derived from reanalysis and satellite observations. Various meteorological fields are derived from daily mean output from the European Centre for Medium-Range Weather Forecasts interim reanalysis (ERA-Interim; Simmons et al. 2007) and are examined over the 1979–2008 period used for the SST boundary conditions in the COOKIE experiments.

Cloud fraction data are obtained from the GCM-Oriented *CALIPSO* Cloud Product (*CALIPSO*-GOCCP; Chepfer et al. 2010) and are examined over the 2007–09 period. To make more direct comparisons to the *CALIPSO*-GOCCP observations, the IPSL model was run with a *CALIPSO* simulator (Chepfer et al. 2008) to simulate the cloud amount that would be observed by the *CALIPSO* satellite from space if it was flying above the model atmosphere.

Cloud radiative effects are estimated from the Clouds and the Earth's Radiant Energy Systems (CERES) Energy Balanced and Filled (EBAF) Ed2.8 data product (Loeb et al. 2009), and are examined over the period 2001–13.

c. Diagnostic approach

The following diagnostic tools are used to characterize and interpret the impacts of ACRE on the atmospheric circulation.

The static stability (N^2) is defined as $g\theta^{-1}\partial\theta/\partial z$, where g is 9.81 m s^{-2} and θ is potential temperature, and tropopause height is identified using the World Meteorological Organization lapse rate definition. The zonal-mean eddy kinetic energy (EKE) is defined as $0.5[u^{*2} + v^{*2}]$, the zonal-mean eddy fluxes of momentum as $[u^*v^*]$, and the zonal-mean eddy fluxes of heat as $[v^*T^*]$, where brackets denote the zonal-mean and the asterisk denotes departures from the zonal mean. The eddy fluxes are calculated first from daily-mean output and then averaged over all days in the integration.

The Eady growth rate provides a quantitative estimate of the growth rate of baroclinic eddies (Lindzen and Farrell 1980; Hoskins and Valdes 1990) and is defined as

$$\sigma_D = 0.31g\frac{1}{N}\frac{1}{T}\left|\frac{\partial T}{\partial y}\right|, \tag{1}$$

where N is the Brunt–Väisälä frequency, a measure of static stability, and $|\partial T/\partial y|$ meridional temperature gradient. The Eady growth rate measures the baroclinicity of the flow and thus the potential energy available for the growth of extratropical storms. The relative contribution of $|\partial T/\partial y|$ to the total changes in the Eady growth rate between the clouds-on and clouds-off simulations was found by setting N to its clouds-on value in the calculation, and the relative contribution of N by setting $|\partial T/\partial y|$ to its clouds-on value.

3. The long-term mean atmospheric circulation and atmospheric cloud radiative effects in the clouds-on experiment

a. The atmospheric circulation in the clouds-on experiment

Figure 1 reviews the latitude–height structure of the zonal-mean circulation from the IPSL model in the control clouds-on experiment. The results are averaged over all 30 years (1979–2008) of the integration. They

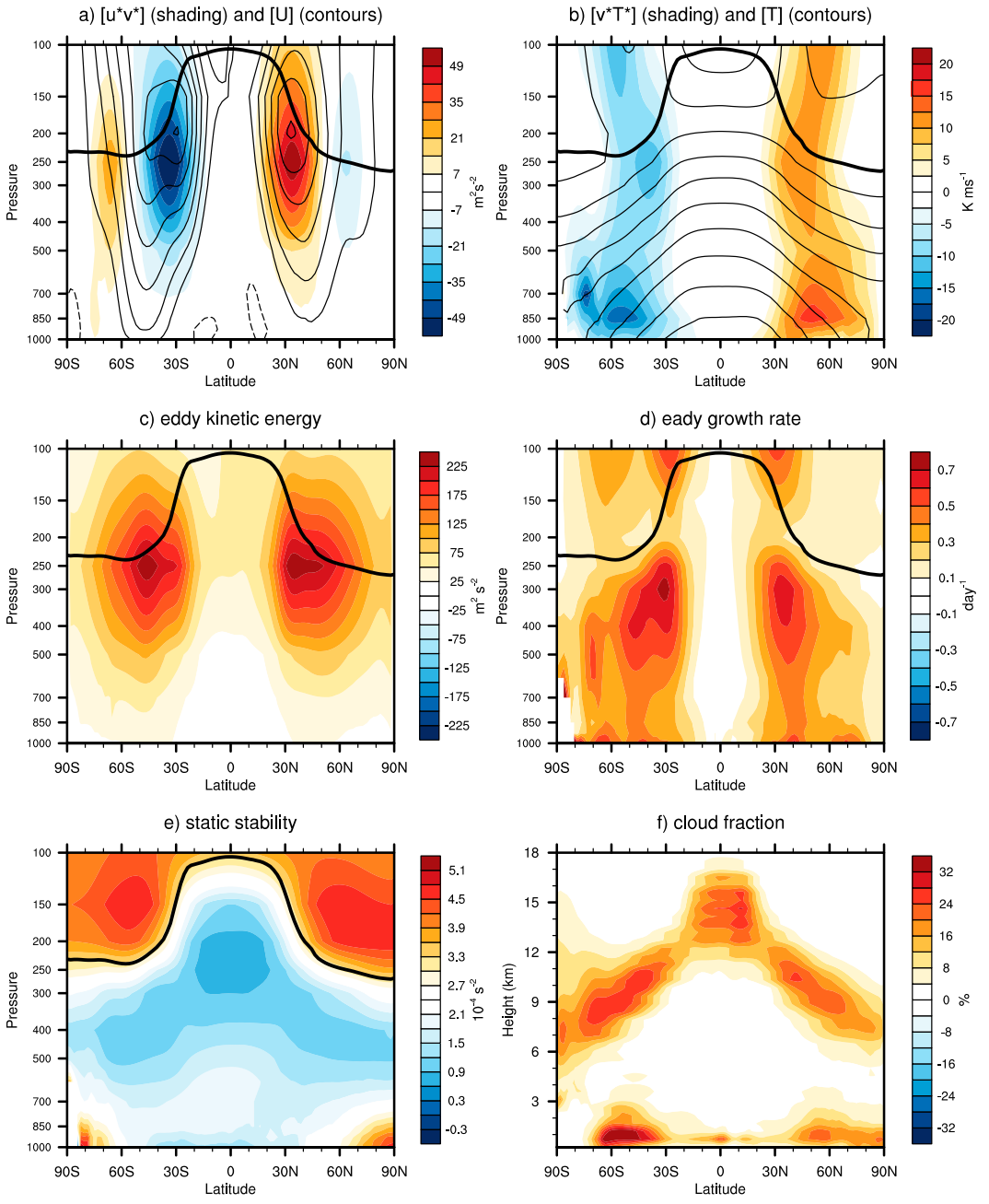

FIG. 1. (a)–(f) The long-term-mean, zonal-mean circulation of the clouds-on experiment for the fields indicated. The cloud fraction data in (f) are derived from model output using the *CALIPSO* simulator. The contour intervals are 5 m s^{-1} in (a) and 10 K in (b). The thick solid line superimposed on each panel indicates the long-term mean tropopause height. In all results, long-term mean denotes the mean over all 30 years of the integration except for the cloud fraction, for which only years 1979 and 1980 are available.

are shown to provide context for the effects of ACRE on the model circulation, as discussed in the following section.

The predominant features in the long-term mean control (clouds on) circulation include the following:

- large meridional temperature gradients and pronounced westerlies in the subtropical upper troposphere (contours in Figs. 1a and 1b);
- surface westerlies at midlatitudes and easterlies in the tropics (contours in Fig. 1a) consistent with the role of

eddy fluxes of momentum in the upper troposphere in driving the surface wind (shading in Fig. 1a);
- maxima in the eddy fluxes of heat near the surface at about 50° latitude and near 250 hPa at about 40° latitude (shading in Fig. 1b);
- large maxima in zonal-mean eddy kinetic energy centered near 250 hPa between 30° and 60° latitude (Fig. 1c), and the maxima in eddy kinetic energy lie immediately above the maxima in the region of largest baroclinic wave growth (i.e., the Eady growth rate; Fig. 1d);
- a minimum in zonal-mean static stability in the tropical upper troposphere and paired maxima in the extratropical lower stratosphere (Fig. 1e; the extratropical maxima are consistent with the tropopause inversion layer, Birner 2006); and
- a maximum in cloud fraction in the upper tropical troposphere consistent with deep convection, minima in cloud fraction in the subtropics consistent with the descending branch of the Hadley cell, maxima in cloud fraction in the midlatitude troposphere consistent with extratropical cyclones, and a maximum in low-level clouds over the Southern Ocean. As noted in section 2b, the distribution of clouds in the model is generated by applying the *CALIPSO* simulator to the model output (Chepfer et al. 2008).

Figure 2 shows the corresponding fields from observations. For the most part, the atmospheric circulation in the control simulation (Figs. 1a–e) bears a strong resemblance to the observations (Figs. 2a–e). Differences include (see also Hourdin et al. 2006) the following: 1) the extratropical westerlies in the IPSL model are shifted equatorward relative to observations (contours in Figs. 1a and 2a); 2) the extratropical baroclinicity (as measured by the Eady growth rate) is larger in the model than in observations (Figs. 1d and 2d); and 3) the region of high static stability just above the extratropical tropopause is less pronounced in the model than in observations.

In terms of the modeled and observed distributions of clouds, the latitude–height structure of cloud fraction diagnosed from the model output (Fig. 1f) bears a resemblance to the observed structure (Fig. 2f). But the amplitudes are notably different. As is the case with other GCMs (e.g., Cesana and Chepfer 2012; Nam et al. 2012), the model overestimates the amount of low clouds in the extratropics, underestimates the amount of low- and midlevel clouds in the tropics, and overestimates the amount of high clouds at middle and high latitudes. The influence of clouds on the general circulation is not related to the cloud fraction per se, but to its impact on cloud radiative effects. The observed and simulated atmospheric cloud radiative effects are compared below.

b. *Atmospheric cloud radiative effects in the clouds-on experiment*

Figure 3 compares the zonal-mean, vertically averaged ACRE derived from the clouds-on control experiment with observations derived from CERES-EBAF. In the tropics and at midlatitudes, the model ACRE are very similar to the observed ACRE. Poleward of 60° latitude, however, the model underestimates the cloud-radiative cooling by a factor of approximately 2, because of either the overestimation of upper-level clouds or the underestimation of low-level clouds, or both (Figs. 1f and 2f).

Figure 4 shows the latitude/height structure of the long-term-mean, zonal-mean, cloud-induced radiative heating rates in the clouds-on experiment. Figure 4a shows the longwave component, Fig. 4b the shortwave component, and Fig. 4c the total heating rates. At all levels, the cloud-induced radiative heating rates are defined as the difference between the all-sky and clear-sky radiative heating rates, and thus represent the perturbation of the radiative heating rates induced by the model clouds.

The cloud-induced longwave radiative heating rates are about 3–4 times larger than the shortwave heating rates, in agreement with results shown in observational studies (Kato et al. 2008; Allan 2011; Haynes et al. 2013). The cloud-induced total radiative heating rates (Fig. 4c) have a distinct latitude/height structure. The radiative effects of clouds are positive in the middle troposphere but negative in the upper troposphere near the tropopause level. The regions of positive cloud radiative effects are due to the trapping of outgoing longwave radiation by middle- and upper-level clouds; negative cloud radiative effects are found at the top of clouds, due to the fact that the longwave emission by cloud tops exceeds that incident from above. The heating of the middle troposphere is larger in the tropics than in the polar regions, likely due to the larger optical depth of clouds in the tropics (Kato et al. 2008).

In the lower troposphere, the net atmospheric radiative effect of clouds is negative in the boundary layer atmosphere but positive near the surface (the heating near the surface is not shown in the figure). At middle and high latitudes, the negative radiative forcing in the boundary layer is larger than the positive radiative forcing in the middle troposphere. Hence, as noted in observations in Kato et al. (2008), Allan (2011), and Haynes et al. (2013), the vertically integrated cloud radiative effect within the atmosphere is negative at middle and high latitudes (also see Fig. 3).

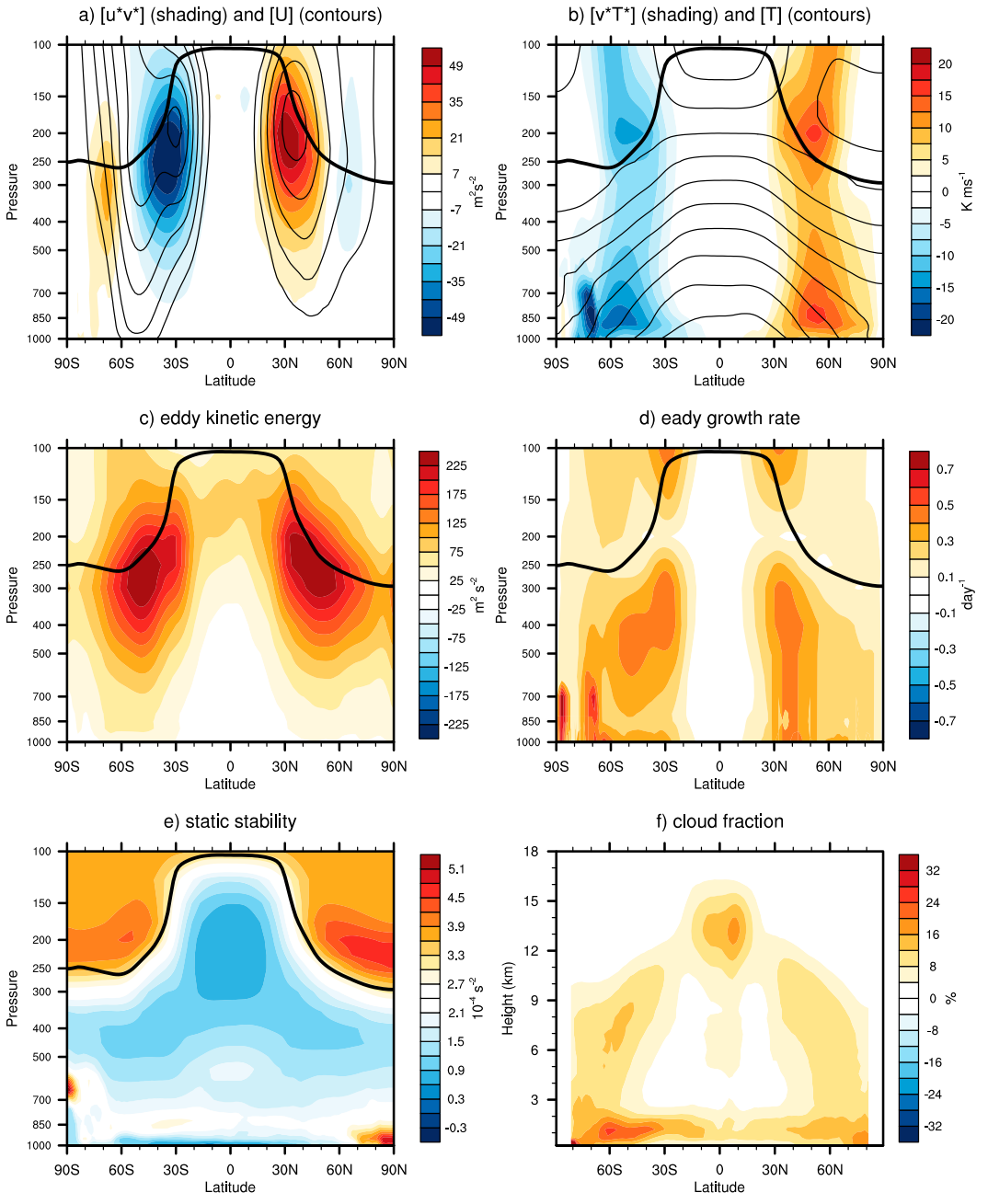

FIG. 2. (a)–(e) As in Figs. 1a–e, but for the corresponding fields derived from the ERA-Interim averaged over the period 1979–2008. (f) As in Fig. 1f, but for the cloud fraction derived from *CALIPSO*-GOCCP averaged over 2007–09.

4. The influence of atmospheric cloud radiative effects on the large-scale atmospheric circulation

In this section we document the response of the zonal-mean atmospheric circulation to the atmospheric cloud radiative effects shown in Fig. 4c. To do so, we examine the differences in the long-term-mean, zonal-mean atmospheric circulation in the IPSL model between the 30-yr clouds-on and clouds-off experiments. The mechanisms of the response are explored in section 5.

Figures 5–8 explore the impacts of ACRE on the zonal-mean, long-term-mean atmospheric circulation. As noted above, the effects of ACRE are given by the differences between the clouds-on and clouds-off experiments. The statistical significance of the differences is assessed using a two-tailed test of the Student's t statistic for

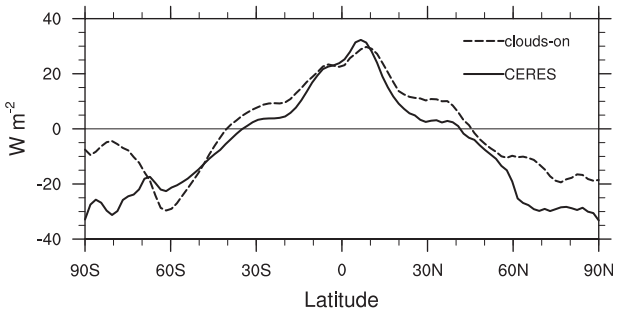

FIG. 3. The long-term-mean, zonal-mean, vertically integrated atmospheric cloud radiative effects in the clouds-on experiment (dashed line) and CERES-EBAF observations (solid line).

the difference of means, where we assume there are 2 degrees of freedom in each calendar year.

Figure 5 examines the influences of ACRE on the zonal-mean temperature, wind, and eddy kinetic energy fields. In all fields, the response to ACRE exhibits a high degree of hemispheric symmetry. The primary features include the following:

- Cooling in the extratropical lower stratosphere/upper troposphere that peaks around 200 hPa and 55° latitude, juxtaposed against warming in the free troposphere that peaks around 200 hPa at the equator (Fig. 5a). The warming exceeds 2 K throughout the tropical troposphere and is consistent with the positive ACRE in the middle and upper troposphere (Fig. 4c). The cooling exceeds 5 K throughout much of the extratropical lower stratosphere and lies above the negative ACRE near the tropopause (Fig. 4c). Since the cooling of the extratropical tropopause region is not clearly collocated with the negative ACRE (as shown in Fig. 4c), it must be driven dynamically, as indicated further below.
- Lifting of the tropopause at all latitudes (the heights of the tropopause in the clouds-on and clouds-off experiments are indicated by the solid and dashed lines, respectively). The lifting of the tropopause is consistent with the modified thermal structure of the atmosphere (i.e., warming of the troposphere juxtaposed against cooling of the extratropical upper troposphere–lower stratosphere; Fig. 5a).
- Eastward wind anomalies in the extratropical zonal flow between approximately 30° and 45° latitude juxtaposed against weak (but significant) westward anomalies poleward of approximately 60° (Fig. 5b). The vertical shear of the wind anomalies at upper levels is mandated by the large meridional gradients in temperature at the tropopause level (Fig. 5a). The surface component of the wind anomalies is consistent with the attendant changes in the eddy fluxes of momentum, as discussed below.
- Eastward wind anomalies centered about the equator in the tropical upper troposphere–lower stratosphere region (UTLS; Fig. 5b). Immediately poleward of the equator, the wind anomalies are consistent with the vertical shear of the flow required by the anomalous meridional temperature gradients in the subtropical UTLS. But at the equator, the wind anomalies must be driven by momentum fluxes due to either the mean meridional circulation or eddies (e.g., Dima et al. 2005; Kraucunas and Hartmann 2005; Dima and Wallace 2007). The response of the eastward wind anomalies in the tropical UTLS region will be discussed later in section 5b.

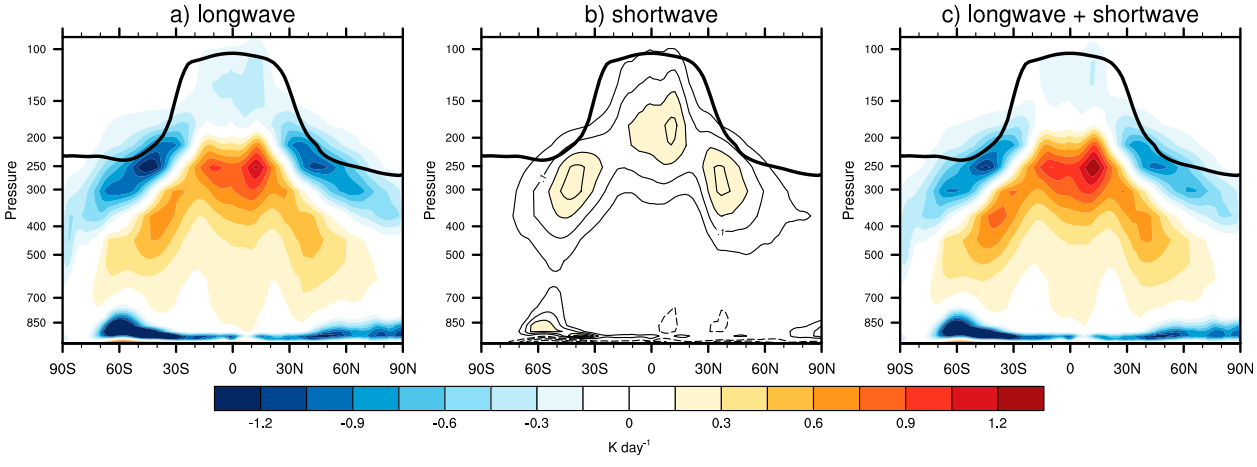

FIG. 4. The long-term-mean, zonal-mean atmospheric cloud radiative effects in the clouds-on experiment: (a) the longwave component, (b) the shortwave component, and (c) the total cloud radiative effects. The contours in (b) are at 0.05 K day^{-1} and are included to help indicate the structure of the relatively weak shortwave forcing. The thick solid line superimposed on each panel indicates the long-term mean tropopause height in the clouds-on experiment.

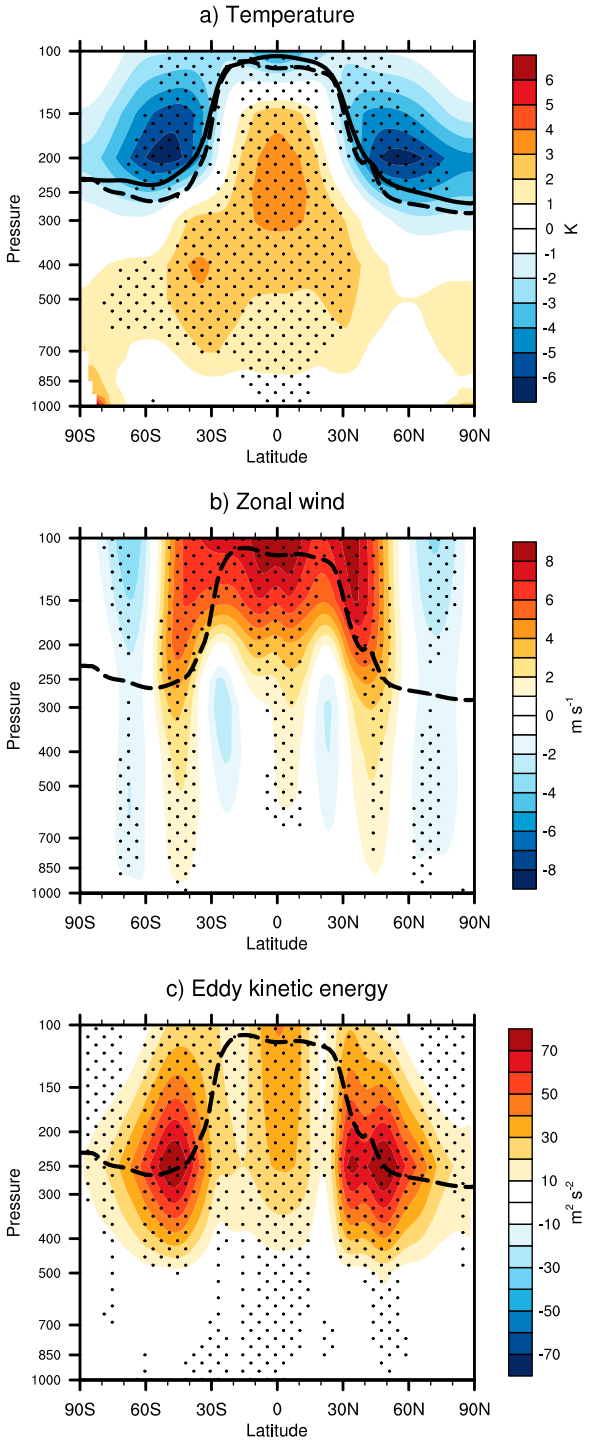

FIG. 5. (a)–(c) Differences in the long-term-mean, zonal-mean atmospheric circulation between the clouds-on and clouds-off experiments for fields indicated. Differences that are significant at the 99% level are stippled. The dashed lines in all panels indicate the long-term mean tropopause height in the clouds-off experiment. The solid line in (a) indicates the long-term mean tropopause height in the clouds-on experiment.

- Widespread increases in EKE centered in both the extratropical and tropical UTLS (Fig. 5c). The changes in extratropical EKE account for about a 30% increase in eddy amplitudes (cf. Figs. 5c and 1c). They project strongly onto the leading pattern of storm track variability documented in Lau (1988) and Wettstein and Wallace (2010) and also onto the positive polarity of the baroclinic annular mode (Thompson and Woodworth 2014a,b).

Figure 6 shows the attendant changes in the fields of the eddy fluxes of momentum (contours in Fig. 6a) and heat (contours in Fig. 6b). The changes in the eddy fluxes are superposed on the changes in the zonal-mean zonal wind (shading in Fig. 6a) and temperature (shading in Fig. 6b) reproduced from Fig. 5. The primary responses in the eddy fluxes again exhibit a high degree of hemispheric symmetry, and include the following:

- Anomalously poleward momentum fluxes centered at approximately 40° juxtaposed against anomalously equatorward momentum fluxes centered at approximately 60° (note that poleward fluxes are denoted by positive values in the Northern Hemisphere but negative values in the Southern Hemisphere). The associated convergence of the eddy flux of eastward momentum between approximately 40° and 60° must drive the anomalous surface eastward flow there; the divergence of the eddy flux of eastward momentum poleward of approximately 60° must drive the anomalous surface westward flow there. The weak eddy momentum fluxes in the tropical UTLS imply convergence of eastward momentum at the equator.
- Anomalously poleward heat fluxes in the upper troposphere and lower stratosphere between approximately 20° and 50° collocated with anomalously equatorward heat fluxes centered around 250 hPa at subpolar latitudes. (The anomalous eddy fluxes of heat are not shown below 500 hPa where they are noisy, amorphous, and uniformly insignificant). The anomalous eddy fluxes of heat are oriented down the gradient of the temperature anomalies and thus can be interpreted as responding to (as opposed to driving) the changes in atmospheric temperature.

Figure 7 shows the associated changes in static stability (Fig. 7a) and cloud fraction (Fig. 7b). As also indicated by the changes in temperature (Fig. 5a), ACRE led to widespread decreases in atmospheric static stability near the tropopause and relatively weak increases in static stability in the extratropical lower stratosphere (the associated changes in tropopause height are reproduced from Fig. 5a). ACRE also led to increases in cloud fraction that peak in the extratropical upper

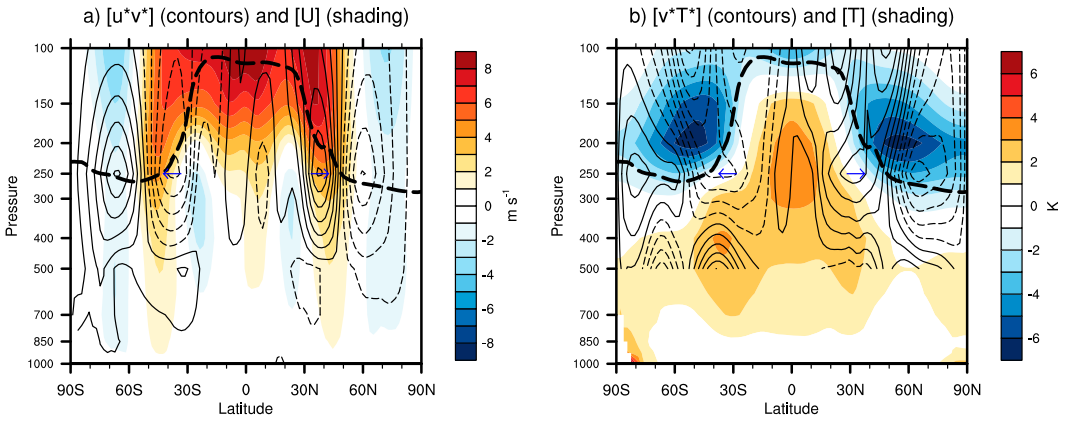

FIG. 6. (a),(b) Differences in the long-term-mean, zonal-mean atmospheric circulation between the clouds-on and clouds-off experiments for fields indicated. The thick dashed lines in all panels indicate the long-term mean tropopause height in the clouds-off experiment. Eddy fluxes of heat below 500 hPa are masked out. Contours start at $\pm 1\,\mathrm{m^2\,s^{-2}}$ with interval of $2\,\mathrm{m^2\,s^{-2}}$ in (a) and $\pm 0.2\,\mathrm{K\,m^{-2}}$ with interval of $0.4\,\mathrm{K\,m^{-2}}$ in (b) and dashed contours denote negative values. Note that the zonal wind in (a) and temperature in (b) are reproduced from Fig. 5. Horizontal arrows near 250 hPa at ~40° indicate the direction of the eddy fluxes.

troposphere (Fig. 7b). The increases in extratropical cloud fraction project strongly onto the decreases in atmospheric static stability, consistent with the linkages between free tropospheric cloud incidence and static stability found in observations (Li et al. 2014a).

Finally, Fig. 8 compares the long-term-mean, zonal-mean precipitation in the clouds-on and clouds-off experiments. In both experiments, the long-term mean precipitation exhibits a maximum in the deep tropics that peaks north of the equator, minima at subtropical latitudes, and maxima in the extratropical storm-track regions, which is in broad agreement with the long-term mean precipitation found in other climate models (Dai 2006; Lin 2007). ACRE led to increases in precipitation at middle-to-high latitudes (indicated by the red shading between 40° and 65°) and decreases at subtropical latitudes (indicated by the blue shading between 20° and 40°). They also lead to decreases in precipitation at tropical latitudes between 20°S and 20°N. Interestingly, similar experiments focusing on the impact of boundary layer cloud radiative effects show that low-cloud radiative effects tend to increase tropical precipitation (Fermepin and Bony 2014). Therefore the results shown here imply that the influence on tropical precipitation of free-tropospheric clouds (which radiatively heat the atmosphere) dominates that of planetary boundary layer clouds (which radiatively cool the atmosphere).

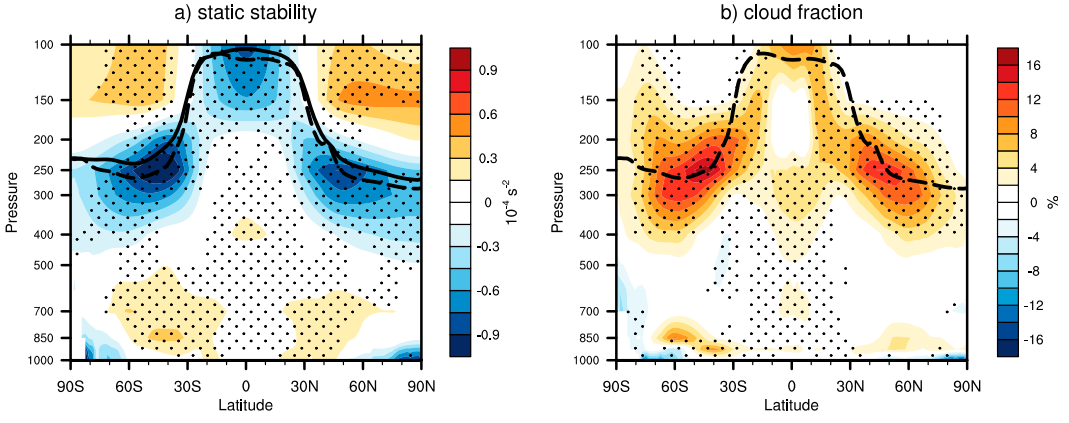

FIG. 7. (a),(b) Differences in the long-term-mean, zonal-mean atmospheric circulation between the clouds-on and clouds-off experiments for fields indicated. Differences that are significant at the 99% level are stippled. The dashed lines in both panels indicate the long-term mean tropopause height in the clouds-off experiment. The solid line in (a) indicates the long-term mean tropopause height in the clouds-on experiment. The cloud fraction data in (b) are the pure model output of cloud amount without a *CALIPSO* simulator.

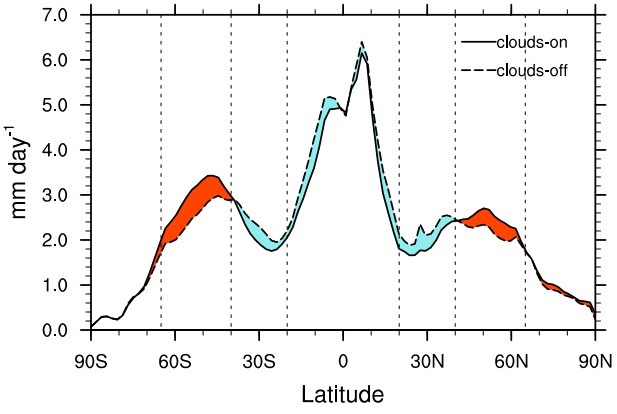

FIG. 8. The meridional structure of the long-term-mean, zonal-mean precipitation in the clouds-on (solid line) and clouds-off (dashed line) experiments. Areas shaded in red indicate regions where precipitation in the clouds-on experiment exceeds that in the clouds-off experiment, and vice versa for areas shaded in blue. Vertical lines are drawn at 20°, 40°, and 65° latitudes for reference.

5. Interpretation

The response of the zonal-mean atmospheric circulation to atmospheric cloud radiative effects is consistent with a series of dynamical and thermodynamical processes. As discussed below, the response of the extratropical atmospheric circulation is consistent with the influence of ACRE on upper tropospheric baroclinicity and the amplitude of baroclinic waves. In the tropics, it is consistent with the influence of ACRE on the amplitude of the equatorial Rossby waves and the energy balance requirements in the free tropical troposphere. We begin with a discussion of the extratropical response.

a. *Extratropical circulation*

The eddy fluxes of momentum and heat play a central role in the extratropical circulation. Both are linked to the amplitudes of midlatitude baroclinic waves: anomalously large amplitude of midlatitude eddies derive from anomalously large poleward fluxes of heat (Holton 2004; Vallis 2006). They can also lead to anomalously large wave fluxes of momentum through the life cycle of baroclinic waves (Simmons and Hoskins 1978; Edmon et al. 1980). The amplitudes of midlatitude eddies, in turn, are closely connected to the amplitude of the extratropical baroclinicity, which provides the fundamental source of energy for developing baroclinic waves. As noted in section 2, the growth rate of developing baroclinic waves can be estimated from the Eady growth rate.

The response of the extratropical atmospheric circulation to ACRE is qualitatively consistent with the changes in baroclinicity and thus wave growth in the extratropical upper troposphere. Figure 9 shows the changes in the extratropical Eady growth rate between the clouds-on and clouds-off experiments. In the extratropical upper troposphere, the amplitude of the Eady growth rate is about 30% larger in the clouds-on experiment than it is in the clouds-off experiment. The response peaks near 300 hPa and at approximately 40°, and is closely collocated with the long-term mean maxima in the Eady growth rate in the clouds-on experiment (see Fig. 1d). The increases

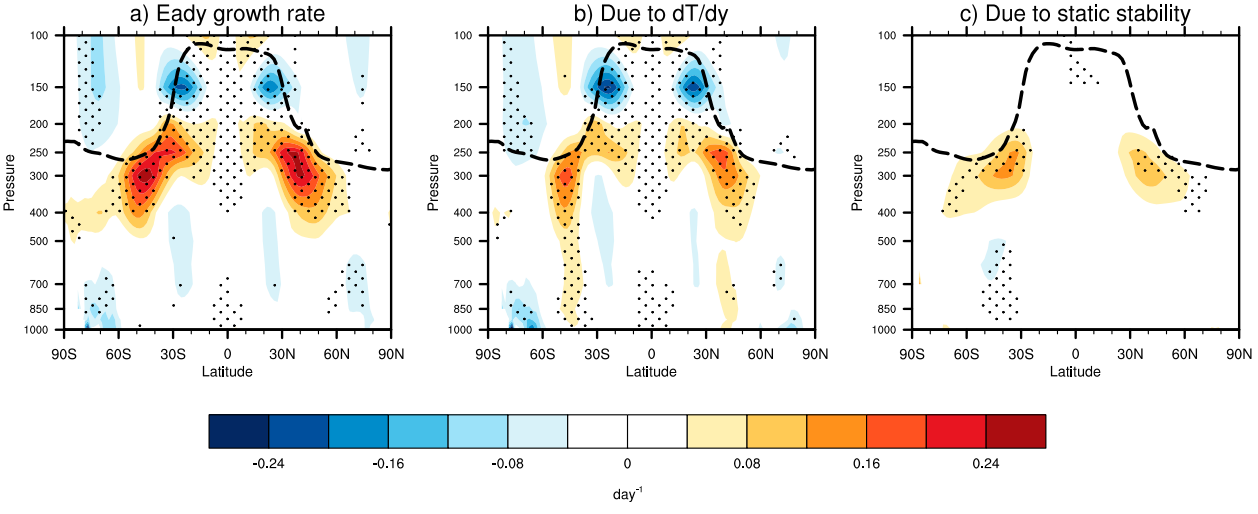

FIG. 9. Differences in the long-term-mean, zonal-mean Eady growth rate between the clouds-on and clouds-off experiments: (a) differences in the total Eady growth rate, (b) differences due to changes in the meridional temperature gradient, and (c) differences due to changes in the static stability. Differences that are significant at the 99% level are stippled. The dashed lines in all panels indicate the long-term mean tropopause height in the clouds-off experiment.

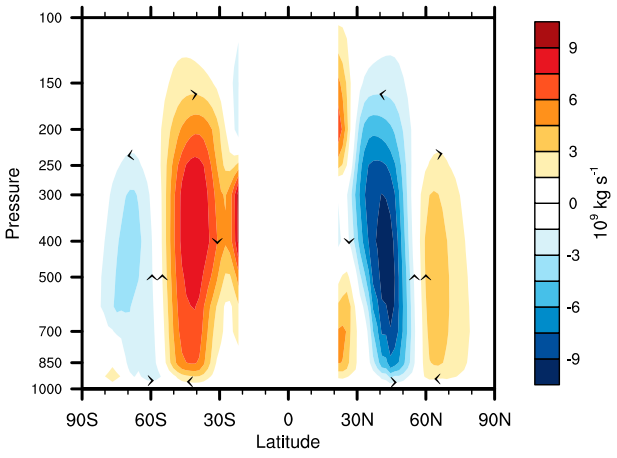

FIG. 10. Differences in the long-term-mean, zonal-mean meridional overturning circulation between the clouds-on and clouds-off experiments. The meridional overturning circulation is shown as the zonal-mean mass streamfunction. Results are masked out in the tropics, where the results are spatially amorphous and not significant.

in the Eady growth rate derive from both increases in the meridional temperature gradient [Fig. 9b; the numerator in Eq. (1)] and decreases in the static stability [Fig. 9c; the denominator in Eq. (1)] in the extratropical upper troposphere.

The increases in the Eady growth rate in the extratropical upper troposphere correspond to a destabilization of the extratropical upper troposphere to baroclinic wave growth. The destabilization of the flow is consistent with the increases in the poleward eddy fluxes of heat (Fig. 6b) and eddy kinetic energy (Fig. 5c) at middle latitudes; that is, regions where the flow is more baroclinically unstable are marked by both anomalously poleward fluxes of heat by atmospheric eddies and enhanced eddy amplitudes. The much larger eddy amplitudes are also consistent with enhanced "stirring" of the midlatitude circulation by baroclinic instability. Stirring of the extratropical circulation leads to the generation of Rossby waves in the upper troposphere that propagate meridionally away from—and flux eastward momentum into—the stirring region (Held 2000; Vallis 2006). Hence, the changes in the eddy fluxes of momentum indicated in Fig. 6a are at least qualitatively consistent with the influence of ACRE on the amplitude of baroclinic waves in the extratropical middle and upper troposphere.

The changes in the eddy fluxes of momentum indicated in Fig. 6a, in turn, play a central role in the changes in vertical motion at extratropical latitudes (indicated in Fig. 10). At extratropical latitudes, the zonal-mean (Eulerian) meridional overturning circulation is driven primarily by the eddy fluxes of momentum (Vallis 2006; the fluxes of momentum by the mean meridional flow contribute primarily at low latitudes). For example, eastward forcing due to the convergence of the eddy flux of eastward momentum is balanced by westward forcing due to the Coriolis torque acting on the meridional flow, and vice versa. In the case of the response to ACRE, the anomalous convergence of the eddy flux of eastward momentum in the upper troposphere between approximately 40° and 60° latitude (Fig. 6a) must be balanced in part by the Coriolis torque acting on anomalously equatorward flow. As indicated in Fig. 10, both hemispheres are, in fact, marked by equatorward flow at middle latitudes, consistent with the force balance requirements noted above. Similar reasoning applies to the anomalous divergence of the eddy flux of eastward momentum and poleward flow at subpolar latitudes.

The changes in the meridional motion induced by the eddy fluxes of momentum play an important role in the changes in extratropical precipitation. From continuity of mass, the anomalous meridional flow driven by the momentum fluxes must be accompanied by rising motion centered at approximately 50° and descending motion centered at approximately 30° (Fig. 10). Comparing Figs. 8 and 10, it is clear that regions with anomalous ascending motion at middle-to-high latitudes are closely collocated with regions of increased precipitation, whereas regions with anomalous descending motion at subtropical latitudes are closely collocated with regions of decreased precipitation. Hence, the changes in extratropical precipitation induced by ACRE can be viewed as fundamentally driven by the anomalous eddy momentum fluxes aloft, which in turn are driven by the influence of ACRE on the extratropical upper tropospheric baroclinicity.

b. *Tropical circulation*

In the tropics, the primary influences of ACRE on the zonal-mean atmospheric circulation include 1) eastward wind anomalies in the UTLS and 2) a reduction in precipitation. The former can be traced to increased amplitude of the equatorial planetary waves and the latter to the energetic constraints on large-scale tropical precipitation (e.g., O'Gorman et al. 2012).

The equatorial waves are driven by zonally asymmetric heating in the tropical atmosphere. The prominent latent heating over the western tropical Pacific induces an off-equatorial Rossby wave response to the west of the heating and a Kelvin wave response to the east (e.g., Gill 1980; Highwood and Hoskins 1998; Dima et al. 2005; Dima and Wallace 2007). The equatorial Rossby waves propagate out of the deep tropics and hence flux eastward momentum into the tropical UTLS (Dima et al. 2005; Dima and Wallace 2007).

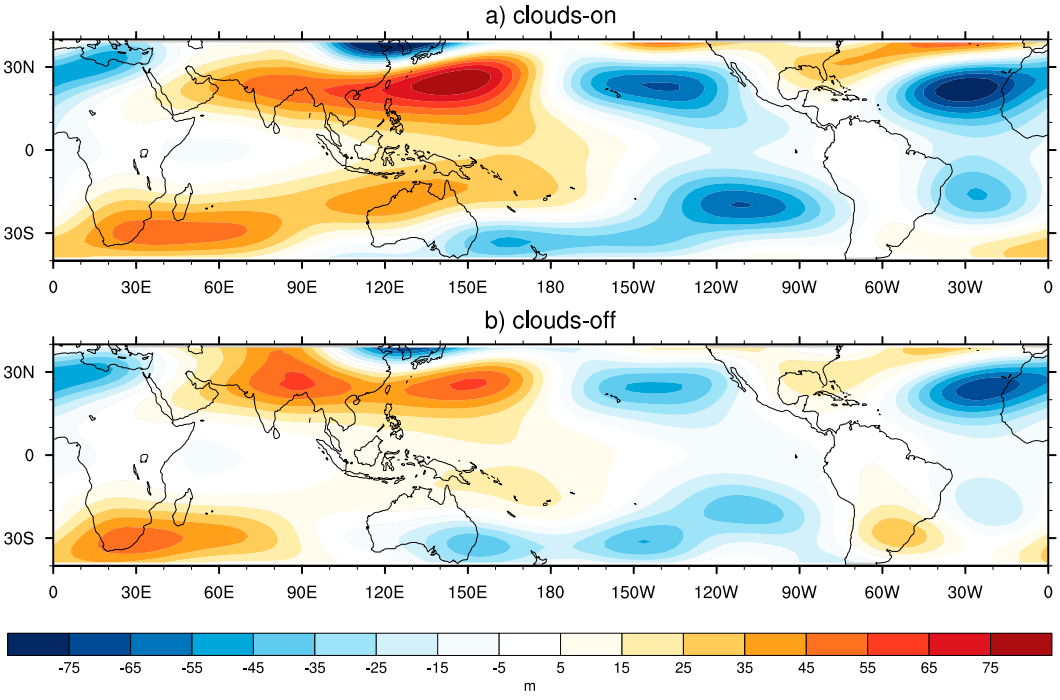

FIG. 11. Horizontal structure of the long-term-mean, 150-hPa height field in the (a) clouds-on and (b) clouds-off experiments. Results show the zonal asymmetric component of the geopotential height at 150 hPa (i.e., the zonal-mean has been removed from the data).

Figure 11 indicates the horizontal structure of the long-term mean 150-hPa geopotential height in the clouds-on (Fig. 11a) and clouds-off (Fig. 11b) experiments. The results show the wave component of the 150 hPa geopotential height field (i.e., the geopotential height field minus its zonal mean). ACRE evidently play a key role in governing the structure of the geopotential height field at 150 hPa. In the clouds-on experiment, the 150-hPa geopotential height field is characterized by paired off-equatorial ridges centered at about 120°–160°E and troughs centered at about 110°–150°W. The structure of the tropical 150-hPa geopotential height field in the clouds-on experiment is qualitatively similar to that in the observations (Dima et al. 2005; Dima and Wallace 2007) [cf. Fig. 1b in Grise and Thompson (2012)]. In the clouds-off experiment, the amplitudes of the off-equatorial ridges and troughs are notably weaker than they are in the clouds-on experiment. The results in Fig. 11 imply that observed equatorial waves are affected not only by latent heating but also the associated cloud-induced radiative heatings. The more pronounced structure of the equatorial planetary waves is consistent with the increases in tropical eddy kinetic energy (Fig. 5c), the anomalous equatorward flux of eastward momentum (Fig. 6a), and the anomalous eastward wind anomalies (Fig. 5b) in the tropical upper UTLS found in association with the ACRE.

The signature of ACRE on tropical precipitation is not clearly attributable to changes in zonal-mean vertical motion (not shown; the changes in tropical vertical motion are noisy and not significant). Rather they are consistent with the energetic constraints on tropical precipitation [see review by O'Gorman et al. (2012), and references therein]. As discussed in section 2a, the COOKIE experiment design is useful for understanding behaviors constrained by the atmospheric energy budget, including precipitation (e.g., Mitchell et al. 1987). On large spatial scales, the changes in precipitation are constrained by changes in 1) the radiative cooling of the atmosphere and 2) the surface sensible heat flux. Averaged over the tropics (30°S–30°N), the changes in the vertically integrated radiative heating between the clouds-on and clouds-off experiments is $+13.3\,\mathrm{W\,m^{-2}}$, which is the sum of the changes in the clear-sky radiative cooling ($\Delta R_{\mathrm{clear}} = -4.6\,\mathrm{W\,m^{-2}}$) and the atmospheric cloud radiative effect ($\Delta\mathrm{ACRE} = 17.9\,\mathrm{W\,m^{-2}}$). The increases in clear-sky radiative cooling are dominated by the increases in longwave radiative cooling of the atmosphere to the surface, and are due to both higher atmospheric temperatures and increases in water vapor in the clouds-on experiment compared to the clouds-off

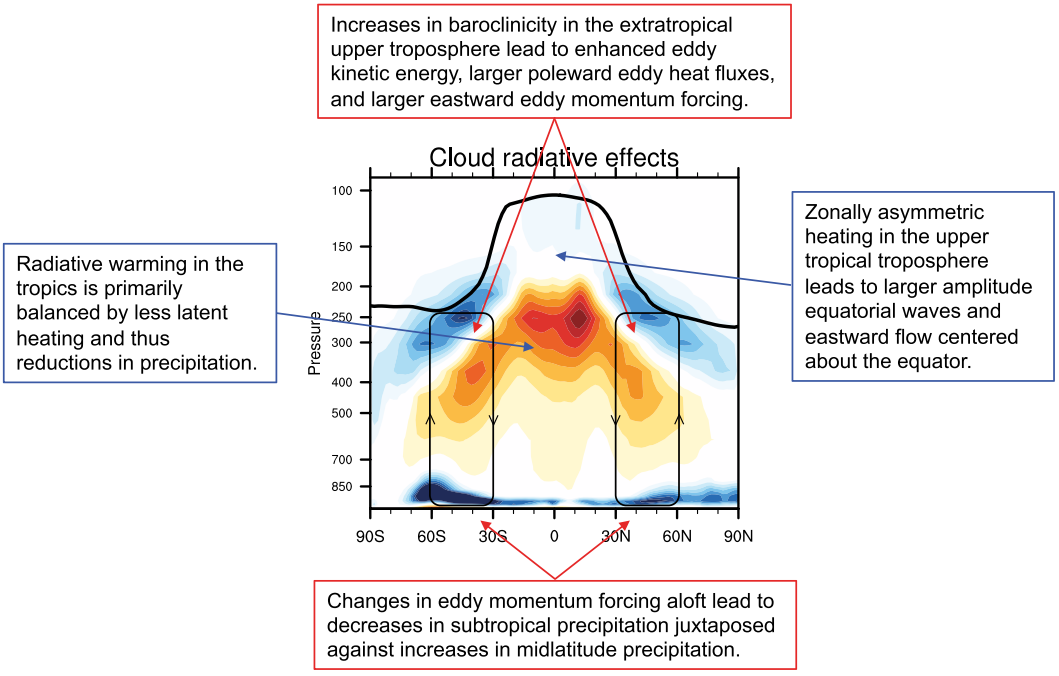

FIG. 12. Schematic diagram summarizing the basic impacts of cloud radiative effects on the zonal-mean circulation, as revealed in this study. The shading is reproduced from Fig. 4c and indicates the cloud radiative effects in the clouds-on experiment; the solid line indicates the long-term mean tropopause height from the clouds-on experiment.

experiment (e.g., Allan 2006; Stephens and Ellis 2008; Philipona et al. 2009; O'Gorman et al. 2012). The heating by the radiative effects of clouds in the clouds-on experiment ($+13.3\,\mathrm{W\,m^{-2}}$) is balanced by reductions (relative to the clouds-off experiment) in 1) the latent heating of condensation ($L\Delta P = -8.9\,\mathrm{W\,m^{-2}}$) and 2) the upward surface sensible heat flux ($\Delta\mathrm{SH} = -3.7\,\mathrm{W\,m^{-2}}$). Here fluxes into the atmosphere are defined as positive. Hence the heating of the tropical atmosphere by ACRE (Fig. 4c) is primarily balanced by a reduction in the latent heating, consistent with the reduction in tropical precipitation evident in the clouds-on simulation (Fig. 8).

6. Summary and discussion

As summarized in Fig. 12, atmospheric cloud radiative effects impact the atmospheric circulation in several ways. They lead to the following:

1) Increases in baroclinicity and eddy activity in the extratropical upper troposphere; as discussed in section 5, the increases in baroclinicity are physically consistent with increases in the kinetic energy, poleward fluxes of heat, and eastward momentum forcing associated with eddies in the midlatitude upper troposphere. The changes in eddy momentum forcing, in turn, drive a dipole in the zonal-mean zonal wind anomalies, with anomalous eastward flow centered at approximately 45° and anomalous westward flow at subtropical latitudes. They also drive changes in vertical motion that subsequently lead to increases in precipitation at middle-to-high latitudes (40°–65°) and decreases in the subtropics (20°–40°).
2) Eastward flow in the tropical UTLS region; the eastward flow is consistent with the influence of the zonally asymmetric structure of the tropical ACRE on the amplitude of the equatorial planetary waves.
3) Decreases in tropical precipitation; the decreases in tropical precipitation are consistent with a reduction in tropical tropospheric latent heating, which is required to balance the radiative heating due to ACRE there.

We have focused on the atmospheric response to ACRE imposed at all levels and latitudes. We tested whether the primary changes found in this study are due to clouds in the planetary boundary layer by examining atmospheric circulation response in COOKIE experiments in which only the radiative effects of boundary layer clouds are turned off (see section 2a). Preliminary results (not shown) indicate that the notable changes in tropospheric eddy activity shown here are not simulated in those experiments. Hence the effects on the

atmospheric circulation of planetary boundary layer clouds are seemingly smaller than the effects on the circulation of free tropospheric clouds.

We also tested the results in the aquaplanet configuration of the IPSL model, and found changes in tropospheric eddy activity similar to those documented here (not shown). Hence, despite the fact that land surface temperature can change in the clouds-off experiments (land surface temperatures are not prescribed), the effects of changes in land surface temperatures on the atmospheric circulation are secondary compared to those associated with changes in the atmospheric diabatic heating (see also Fermepin and Bony 2014). The results based on the aquaplanet simulations also confirm that the unique land–sea geometry of a particular hemisphere does not play a key role in the zonal-mean responses examined here.

The findings shown here highlight the key role of ACRE in determining the structure of the large-scale atmospheric circulation. The results are derived from a single AGCM (the IPSL-CM5A-LR). We also tested the results in the other atmospheric component of the IPSL model (i.e., IPSL-CM5B-LR) and found changes in tropospheric eddy activity similar to those documented here (not shown). The amplitude of the circulation response might be overestimated by the IPSL model as it overestimates the meridional gradient in ACRE at midlatitudes (see Fig. 3). But since the response mechanisms follow from a series of physically consistent relationships, we expect they will prove robust in any climate model that predicts roughly the same latitude–altitude structure of ACRE as that shown in Fig. 4c.

The results have two primary implications for climate modeling. One, they make clear that model biases in tropospheric cloud radiative effects lead to bias not only in Earth's radiation budget and the tropical atmospheric flow but also the extratropical circulation, even with realistic SSTs. They hence reveal that cloud radiative effects bias the extratropical circulation not only through their shortwave impacts on the meridional gradients in SST (Ceppi et al. 2012) but also through their influence on the thermal structure of the atmosphere. Two, they suggest that uncertainties in the response of clouds to climate change depend not only on the shortwave radiative effects of clouds on SSTs (Ceppi et al. 2014; Grise and Polvani 2014) but also on the longwave radiative effects of clouds on atmospheric heating rates and temperature (see also Voigt and Shaw 2015).

The findings raise several obvious questions for future work. For example: What is the relative role of tropical and extratropical cloud radiative effects in driving the extratropical atmospheric response indicated here? Is the atmospheric response to atmospheric cloud radiative effects robust in other climate models? How does the atmospheric response vary as a function of the seasonal cycle? What is the zonally varying structure of the atmospheric response? And to what extent do changes in the cloud radiative effects impact the time scales and structures of large-scale patterns of atmospheric variability? We are exploring these questions in our ongoing analyses.

Acknowledgments. We thank Abderrahmane Idelkadi (LMD) for running the "clouds-off" simulation. YL is funded by CloudSAT via NASA JPL and the NSF Climate Dynamics program. DWJT is funded by the NSF Climate Dynamics program.

REFERENCES

Allan, R. P., 2006: Variability in clear-sky longwave radiative cooling of the atmosphere. *J. Geophys. Res.,* **111,** D22105, doi:10.1029/2006JD007304.

——, 2011: Combining satellite data and models to estimate cloud radiative effect at the surface and in the atmosphere. *Meteor. Appl.,* **18,** 324–333, doi:10.1002/met.285.

Birner, T., 2006: Fine-scale structure of the extratropical tropopause region. *J. Geophys. Res.,* **111,** D04104, doi:10.1029/2005JD006301.

Bony, S., and K. A. Emanuel, 2005: On the role of moist processes in tropical intraseasonal variability: Cloud–radiation and moisture–convection feedbacks. *J. Atmos. Sci.,* **62,** 2770–2789, doi:10.1175/JAS3506.1.

——, G. Bellon, D. Klocke, S. Sherwood, S. Fermepin, and S. Denvil, 2013: Robust direct effect of carbon dioxide on tropical circulation and regional precipitation. *Nat. Geosci.,* **6,** 447–451, doi:10.1038/ngeo1799.

Bretherton, C. S., and D. S. Battisti, 2000: An interpretation of the results from atmospheric general circulation models forced by the time history of the observed sea surface temperature distribution. *Geophys. Res. Lett.,* **27,** 757–770, doi:10.1029/1999GL010910.

Ceppi, P., Y.-T. Hwang, D. M. W. Frierson, and D. L. Hartmann, 2012: Southern Hemisphere jet latitude biases in CMIP5 models linked to shortwave cloud forcing. *Geophys. Res. Lett.,* **39,** L19708, doi:10.1029/2012GL053115.

——, M. D. Zelinka, and D. L. Hartmann, 2014: The response of the Southern Hemispheric eddy-driven jet to future changes in shortwave radiation in CMIP5. *Geophys. Res. Lett.,* **41,** 3244–3250, doi:10.1002/2014GL060043.

Cesana, G., and H. Chepfer, 2012: How well do climate models simulate cloud vertical structure? A comparison between *CALIPSO*-GOCCP satellite observations and CMIP5 models. *Geophys. Res. Lett.,* **39,** L20803, doi:10.1029/2012GL053153.

Chepfer, H., S. Bony, D. Winker, M. Chiriaco, J.-L. Dufresne, and G. Séze, 2008: Use of *CALIPSO* lidar observations to evaluate the cloudiness simulated by a climate model. *Geophys. Res. Lett.,* 35, L15704, doi:10.1029/2008GL034207.

——, ——, ——, G. Cesana, J. L. Dufresne, P. Minnis, C. J. Stubenrauch, and S. Zeng, 2010: The GCM-Oriented *CALIPSO*

Cloud Product (*CALIPSO*-GOCCP). *J. Geophys. Res.,* **115,** D00H16, doi:10.1029/2009JD012251.

Crueger, T., and B. Stevens, 2015: The effect of atmospheric radiative heating by clouds on the Madden–Julian oscillation. *J. Adv. Model. Earth Syst.,* **7,** 854–864, doi:10.1002/2015MS000434.

Dai, A., 2006: Precipitation characteristics in eighteen coupled climate models. *J. Climate,* **19,** 4605–4630, doi:10.1175/JCLI3884.1.

Deser, C., and A. S. Phillips, 2009: Atmospheric circulation trends, 1950–2000: The relative roles of sea surface temperature forcing and direct atmospheric radiative forcing. *J. Climate,* **22,** 396–413, doi:10.1175/2008JCLI2453.1.

Dima, I. M., and J. M. Wallace, 2007: Structure of the annual-mean equatorial planetary waves in the ERA-40 reanalyses. *J. Atmos. Sci.,* **64,** 2862–2880, doi:10.1175/JAS3985.1.

——, ——, and I. P. Kraucunas, 2005: Tropical angular momentum balance in the NCEP reanalyses. *J. Atmos. Sci.,* **62,** 2499–2513, doi:10.1175/JAS3486.1.

Dufresne, J.-L., and Coauthors, 2013: Climate change projections using the IPSL-CM5 Earth system model: From CMIP3 to CMIP5. *Climate Dyn.,* **40,** 2123–2165, doi:10.1007/s00382-012-1636-1.

Edmon, H. J., B. J. Hoskins, and M. E. McIntyre, 1980: Eliassen-Palm cross sections for the troposphere. *J. Atmos. Sci.,* **37,** 2600–2616, doi:10.1175/1520-0469(1980)037<2600:EPCSFT>2.0.CO;2.

Fermepin, S., and S. Bony, 2014: Influence of low-cloud radiative effects on tropical circulation and precipitation. *J. Adv. Model. Earth Syst.,* **6,** 513–526, doi:10.1002/2013MS000288.

Fuchs, Z., and D. J. Raymond, 2002: Large-scale modes of a nonrotating atmosphere with water vapor and cloud–radiation feedbacks. *J. Atmos. Sci.,* **59,** 1669–1679, doi:10.1175/1520-0469(2002)059<1669:LSMOAN>2.0.CO;2.

Gill, A. E., 1980: Some simple solutions for heat-induced tropical circulation. *Quart. J. Roy. Meteor. Soc.,* **106,** 447–462, doi:10.1002/qj.49710644905.

Gordon, C., 1992: Comparison of 30-day integrations with and without cloud-radiation interaction. *Mon. Wea. Rev.,* **120,** 1244–1277, doi:10.1175/1520-0493(1992)120<1244:CODIWA>2.0.CO;2.

Grise, K. M., and D. W. J. Thompson, 2012: Equatorial planetary waves and their signature in atmospheric variability. *J. Atmos. Sci.,* **69,** 857–874, doi:10.1175/JAS-D-11-0123.1.

——, and L. M. Polvani, 2014: Southern Hemisphere cloud dynamics biases in CMIP5 models and their implications for climate projections. *J. Climate,* **27,** 6074–6092, doi:10.1175/JCLI-D-14-00113.1.

——, ——, G. Tselioudis, Y. Wu, and M. D. Zelinka, 2013: The ozone hole indirect effect: Cloud-radiative anomalies accompanying the poleward shift of the eddy-driven jet in the Southern Hemisphere. *Geophys. Res. Lett.,* **40,** 3688–3692, doi:10.1002/grl.50675.

Harrison, E. F., P. Minnis, B. R. Barkstrom, V. Ramanathan, R. D. Cess, and G. G. Gibson, 1990: Seasonal variation of cloud radiative forcing derived from the Earth Radiation Budget Experiment. *J. Geophys. Res.,* **95,** 18 687–18 703, doi:10.1029/JD095iD11p18687.

Hartmann, D. L., M. Ockert-Bell, and M. L. Michelsen, 1992: The effect of cloud type on Earth's energy balance: Global analysis. *J. Climate,* **5,** 1281–1304, doi:10.1175/1520-0442(1992)005<1281:TEOCTO>2.0.CO;2.

Haynes, J. M., T. H. V. Haar, T. L'Ecuyer, and D. Henderson, 2013: Radiative heating characteristics of Earth's cloudy atmosphere from vertically resolved active sensors. *Geophys. Res. Lett.,* **40,** 624–630, doi:10.1002/grl.50145.

Held, I. M., 2000: The general circulation of the atmosphere. *Proc. 2000 Program on Geophysical Fluid Dynamics,* Woods Hole, MA, Woods Hole Oceanographic Institution, 66 pp. [Available online at http://www.gfdl.noaa.gov/cms-filesystem-action/user_files/ih/lectures/woods_hole.pdf.]

Highwood, E. J., and B. J. Hoskins, 1998: The tropical tropopause. *Quart. J. Roy. Meteor. Soc.,* **124,** 1579–1604, doi:10.1002/qj.49712454911.

Holton, J. R., 2004: *An Introduction to Dynamic Meteorology.* 4th ed. Academic Press, 535 pp.

Hoskins, B. J., and P. J. Valdes, 1990: On the existence of storm-tracks. *J. Atmos. Sci.,* **47,** 1854–1864, doi:10.1175/1520-0469(1990)047<1854:OTEOST>2.0.CO;2.

Hourdin, F., and Coauthors, 2006: The LMDZ4 general circulation model: Climate performance and sensitivity to parametrized physics with emphasis on tropical convection. *Climate Dyn.,* **27,** 787–813, doi:10.1007/s00382-006-0158-0.

Kato, S., F. G. Rose, D. A. Rutan, and T. P. Charlock, 2008: Cloud effects on the meridional atmospheric energy budget estimated from Clouds and the Earth's Radiant Energy System (CERES) data. *J. Climate,* **21,** 4223–4241, doi:10.1175/2008JCLI1982.1.

——, and Coauthors, 2011: Improvements of top-of-atmosphere and surface irradiance computations with *CALIPSO*-, *CloudSat*-, and MODIS-derived cloud and aerosol properties. *J. Geophys. Res.,* **116,** D19209, doi:10.1029/2011JD016050.

Kraucunas, I. P., and D. L. Hartmann, 2005: Equatorial superrotation and the factors controlling the zonal-mean zonal winds in the tropic. *J. Atmos. Sci.,* **62,** 371–389, doi:10.1175/JAS-3365.1.

Lau, N.-C., 1988: Variability of the observed midlatitude storm tracks in relation to low-frequency changes in the circulation pattern. *J. Atmos. Sci.,* **45,** 2718–2743, doi:10.1175/1520-0469(1988)045<2718:VOTOMS>2.0.CO;2.

L'Ecuyer, T. S., N. B. Wood, T. Haladay, G. L. Stephens, and P. W. Stackhouse, 2008: Impact of clouds on atmospheric heating based on the R04 *CloudSat* fluxes and heating rates data set. *J. Geophys. Res.,* **113,** D00A15, doi:10.1029/2008JD009951.

Lee, M.-I., I.-S. Kang, J.-K. Kim, and B. E. Mapes, 2001: Influence of cloud-radiation interaction on simulating tropical intraseasonal oscillation with an atmospheric general circulation model. *J. Geophys. Res.,* **106,** 14 219–14 233, doi:10.1029/2001JD900143.

Li, Y., D. W. J. Thompson, Y. Huang, and M. Zhang, 2014a: Observed linkages between the northern annular mode/North Atlantic Oscillation, cloud incidence, and cloud radiative forcing. *Geophys. Res. Lett.,* **41,** 1681–1688, doi:10.1002/2013GL059113.

——, ——, G. L. Stephens, and S. Bony, 2014b: A global survey of the linkages between cloud vertical structure and large-scale climate. *J. Geophys. Res. Atmos.,* **119,** 3770–3792, doi:10.1002/2013JD020669.

Lin, J.-L., 2007: The double-ITCZ problem in IPCC AR4 coupled GCMs: Ocean–atmosphere feedback analysis. *J. Climate,* **20,** 4497–4525, doi:10.1175/JCLI4272.1.

Lindzen, R. S., and B. Farrell, 1980: A simple approximate result for the maximum growth rate of baroclinic instabilities. *J. Atmos. Sci.,* **37,** 1648–1654, doi:10.1175/1520-0469(1980)037<1648:ASARFT>2.0.CO;2.

Loeb, N. G., B. A. Wielicki, D. R. Doelling, G. L. Smith, D. F. Keyes, S. Kato, N. Manlo-Smith, and T. Wong, 2009: Toward optimal closure of the Earth's top-of-atmosphere radiation budget. *J. Climate,* **22,** 748–766, doi:10.1175/2008JCLI2637.1.

Mitchell, J. F. B., C. A. Wilson, and W. M. Cunnington, 1987: On CO_2 climate sensitivity and model dependence of results. *Quart. J. Roy. Meteor. Soc.,* **113,** 293–322, doi:10.1002/qj.49711347517.

Möbis, B., and B. Stevens, 2012: Factors controlling the position of the intertropical convergence zone on an aquaplanet. *J. Adv. Model. Earth Syst,* **4,** M00A04, doi:10.1029/2012MS000199.

Nam, C., S. Bony, J.-L. Dufresne, and H. Chepfer, 2012: The 'too few, too bright' tropical low-cloud problem in CMIP5 models. *Geophys. Res. Lett.,* **39,** L21801, doi:10.1029/2012GL053421.

O'Gorman, P. A., R. P. Allan, M. P. Byrne, and M. Previdi, 2012: Energetic constraints on precipitation under climate change. *Surv. Geophys.,* **33,** 585–608, doi:10.1007/s10712-011-9159-6.

Oueslati, B., and G. Bellon, 2013: Convective entrainment and large-scale organization of tropical precipitation: Sensitivity of the CNRM-CM5 hierarchy of models. *J. Climate,* **26,** 2931–2946, doi:10.1175/JCLI-D-12-00314.1.

Philipona, R., K. Behrens, and C. Ruckstuhl, 2009: How declining aerosols and rising greenhouse gases forced rapid warming in Europe since the 1980s. *Geophys. Res. Lett.,* **36,** L02806, doi:10.1029/2008GL036350.

Ramanathan, V., R. D. Cess, E. F. Harrison, P. Minnis, B. R. Barkstrom, E. Ahmad, and D. Hartmann, 1989: Cloud-radiative forcing and climate: Results from the Earth Radiation Budget Experiment. *Science,* **243,** 57–63, doi:10.1126/science.243.4887.57.

Randall, D. A., Harshvardhan, D. A. Dazlich, and T. G. Corsetti, 1989: Interactions among radiation, convection, and large-scale dynamics in a general circulation model. *J. Atmos. Sci.,* **46,** 1943–1970, doi:10.1175/1520-0469(1989)046<1943:IARCAL>2.0.CO;2.

Raymond, D. J., 2001: A new model of the Madden–Julian oscillation. *J. Atmos. Sci.,* **58,** 2807–2819, doi:10.1175/1520-0469(2001)058<2807:ANMOTM>2.0.CO;2.

Sherwood, S. C., V. Ramanathan, T. P. Barnett, M. K. Tyree, and E. Roeckner, 1994: Response of an atmospheric general circulation model to radiative forcing of tropical clouds. *J. Geophys. Res.,* **99,** 20 829–20 845, doi:10.1029/94JD01632.

Simmons, A. J., and B. J. Hoskins, 1978: The life cycles of some nonlinear baroclinic waves. *J. Atmos. Sci.,* **35,** 414–432, doi:10.1175/1520-0469(1978)035<0414:TLCOSN>2.0.CO;2.

——, S. Uppala, D. Dee, and S. Kobayashi, 2007: ERA-Interim: New ECMWF reanalysis products from 1989 onwards. *ECMWF Newsletter,* No. 110, ECMWF, Reading, United Kingdom, 25–35.

Slingo, A., and J. M. Slingo, 1988: The response of a general circulation model to cloud longwave radiative forcing. I: Introduction and initial experiments. *Quart. J. Roy. Meteor. Soc.,* **114,** 1027–1062, doi:10.1002/qj.49711448209.

Slingo, J. M., and A. Slingo, 1991: The response of a general circulation model to cloud longwave radiative forcing. II: Further studies. *Quart. J. Roy. Meteor. Soc.,* **117,** 333–364, doi:10.1002/qj.49711749805.

Stephens, G. L., and T. D. Ellis, 2008: Controls of global-mean precipitation increases in global warming GCM experiments. *J. Climate,* **21,** 6141–6155, doi:10.1175/2008JCLI2144.1.

Stevens, B., and S. Bony, 2013: What are climate models missing? *Science,* **340,** 1053–1054, doi:10.1126/science.1237554.

——, ——, and M. Webb, 2012: Clouds On-Off Klimate Intercomparison Experiment (COOKIE). 12 pp. [Available online at http://www.euclipse.eu/downloads/Cookie.pdf.]

Su, W., A. Bodas-Salcedo, K.-M. Xu, and T. P. Charlock, 2010: Comparison of the tropical radiative flux and cloud radiative effect profiles in a climate model with Clouds and the Earth's Radiant Energy System (CERES) data. *J. Geophys. Res.,* **115,** D01105, doi:10.1029/2009JD012490.

Taylor, K. E., R. J. Stouffer, and G. A. Meehl, 2012: An overview of CMIP5 and the experiment design. *Bull. Amer. Meteor. Soc.,* **93,** 485–498, doi:10.1175/BAMS-D-11-00094.1.

Thompson, D. W. J., and J. D. Woodworth, 2014a: Barotropic and baroclinic annular variability in the Southern Hemisphere. *J. Atmos. Sci.,* **71,** 1480–1493, doi:10.1175/JAS-D-13-0185.1.

——, and ——, 2014b: Periodic variability in the large-scale Southern Hemisphere atmospheric circulation. *Science,* **343,** 641–645, doi:10.1126/science.1247660.

Tian, B., and V. Ramanathan, 2003: A simple moist tropical atmosphere model: The role of cloud radiative forcing. *J. Climate,* **16,** 2086–2092, doi:10.1175/1520-0442(2003)016<2086:ASMTAM>2.0.CO;2.

Vallis, G. K., 2006: *Atmospheric and Oceanic Fluid Dynamics: Fundamentals and Large-Scale Circulation.* Cambridge University Press, 561 pp.

Voigt, A., and T. A. Shaw, 2015: Circulation response to warming shaped by radiative changes of clouds and water vapour. *Nat. Geosci.,* **8,** 102–106, doi:10.1038/ngeo2345.

Wettstein, J., and J. Wallace, 2010: Observed patterns of month-to-month storm-track variability and their relationship to the background flow. *J. Atmos. Sci.,* **67,** 1420–1437, doi:10.1175/2009JAS3194.1.

Zurovac-Jevtić, D., S. Bony, and K. Emanuel, 2006: On the role of clouds and moisture in tropical waves: A two-dimensional model study. *J. Atmos. Sci.,* **63,** 2140–2154, doi:10.1175/JAS3738.1.